Langmuir–Blodgett Monolayers of Long-Chain NBD Derivatives on Silver Island Films: Well-Organized Probe Layer for the Metal-Enhanced Fluorescence Studies

ARTICLE *in* THE JOURNAL OF PHYSICAL CHEMISTRY B · AUGUST 2006

Impact Factor: 3.3 · DOI: 10.1021/jp0620623 · Source: PubMed

3 AUTHORS, INCLUDING:

Ramachandram Badugu

80 PUBLICATIONS **2,491** CITATIONS

SEE PROFILE

Joseph R Lakowicz

University of Maryland Medical Center

877 PUBLICATIONS **42,252** CITATIONS

SEE PROFILE

Langmuir−Blodgett Monolayers of Long-Chain NBD Derivatives on Silver Island Films: Well-Organized Probe Layer for the Metal-Enhanced Fluorescence Studies

Krishanu Ray, Ramachandram Badugu, and Joseph R. Lakowicz*

Center for Fluorescence Spectroscopy, University of Maryland School of Medicine, Department of Biochemistry and Molecular Biology, 725 West Lombard Street, Baltimore, Maryland 21201

Received: April 3, 2006; In Final Form: May 18, 2006

The metal-enhanced fluorescence (MEF) from the well-organized monolayers of two newly prepared long-chain alkylamine derivatives of nitrobenzoxadiazole (NBD-C16 and NBD-C18) deposited on silver island films (SIFs) has been investigated. The NBD derivatives were conveniently prepared by using a single step procedure in quantitative yields. The monolayers of the probes on SIFs as well as on bare-glass slides were obtained by using the Langmuir−Blodgett (LB) technique. Orientation of the NBD probe molecule in LB monolayer film was measured with polarized absorption spectroscopy. The observed tilt angle of the probe transition dipole moment with respect to the surface normal of ∼67−68° was evaluated. We observed that the NBD monolayers deposited in close proximity to silver islands show about a 16-fold increase in fluorescence intensity and shortened fluorescence lifetime compared to those on bare-glass, which are due to metal enhanced fluorescence. On the other hand, the corresponding MEF from randomly oriented film obtained by using spin coating of the probes on SIFs was only 2.5-fold. Further, we deposited mixed monolayers of NBD-C16 or NBD-C18 with various molar ratios of stearic acid to understand the polarity effect on MEF. Interestingly, we found a consistent increase in MEF efficiency with increasing molar ratio of stearic acid. Along with MEF, we also found a continuous blue-shift in emission band maxima of the probes with an increasing molar ratio of stearic acid. The observed increase in MEF efficiency is justified based on cooperative effects of (1) the modulations in electronic density of the surface plasmon absorption band of SIFs and (2) defined probe orientation that might lead to preferential excitation.

Introduction

Over the past several years we have been working on metal enhanced fluorescence (MEF), a newly recognized phenomenon having diversified applications in various fields including chemistry and biology.[1−14] MEF appears to be the result of electromagnetic interactions of the fluorophores at a short distance above the metal surface. These metal−fluorophore interactions lead to important spectral changes, including favorable increases in detectability and brightness (intensity) of fluorophores and photostability, decreased lifetimes due to increased rates of radiative decay, and increased distances for fluorescence resonance energy transfer (FRET).[4,15] Previous research from our laboratory has also shown that fluorophores can create surface plasmons in metals which in turn create light.[4] Surface plasmons are collective oscillations of free electrons in metallic surfaces and particles. These reciprocal fluorophore−metal interactions suggest that it will be possible to control the migration of electromagnetic energy across and through metal surfaces, and to control when and where the energy is converted back into light. We refer to this possibility as plasmon-controlled fluorescence (PCF).[16] Depending on the optical conditions, plasmons created at short fluorophore−metal distances may be trapped at the interface, and as a result they decay as heat.[4,16] Under other conditions the plasmons will radiate the energy from a fluorophore, which appears to occur whenever allowed by the optical conditions. In numerous experiments with fluorophores on silver nanostructures, it has been found that silver island films (SIFs) generally enhance the fluorescence intensity and reduce the lifetime.[1−12] All of these reports have primarily been done with silver nanostructures and immobilizing the fluorophores onto clean glass surfaces and silvered nanostructures. SIFs have a heterogeneous distribution of particle sizes and display characteristic plasmon absorbance.

The application of MEF technology requires a clear understanding of the fluorophore−metal interactions. Most of the previous experiments related to MEF were accomplished by spin casting the fluorophore-doped polymers solutions on the glass or silver island films. In those experiments, there was limited control of the distances between the metal and the fluorophores, and fluorophores were probably present in areas outside the regions where enhanced emission was obtained. Hence, it is not trivial to estimate the enhancement of fluorescence signals from fluorophores deposited on silvered surfaces. The ratio of fluorescence intensities on silvered/glass parts of the substrate is the usual method of estimating the signal enhancement. This enhancement in fluorescence intensity can be due to an increase in pump (excitation) power and/or increased rates of emission.[1,4] However, the magnitude of the MEF may be severely dependent on various experimental conditions including different amounts of fluorophores on the silvered and non-silvered surfaces and the precise distance and orientation of fluorophores with respect to metallic nanostructures. Most of the reports to date assume the presence of equal amounts of fluorophores on metalized and nonmetalized parts of the sample. Traditional absorption spectroscopic measurements are rather difficult and not reliable in estimating the deposited amount of fluorophores on the

* Address correspondence to this author. E-mail: lakowicz@cfs.umbi.umd.edu.

10.1021/jp0620623 CCC: $33.50
Published on Web 06/20/2006

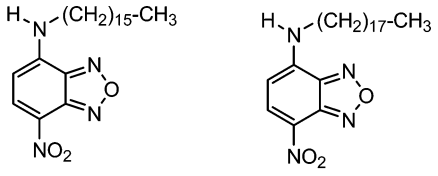

NBD-C16 NBD-C18

Figure 1. Molecular structures of the probes used for LB monolayer preparation.

metalized part of the sample. Controlled amounts of fluorophores deposited on reference (glass) and the sample (metallic) substrate and placing the fluorophores at a well-defined distance and orientation from the metallic nanostructures are the most important factors in measuring the enhanced fluorescence signal in a quantitative manner.

To control the numbers of fluorophores on a substrate and place them at well-defined distances and with certain orientation, we use the Langmuir−Blodgett (LB) film deposition technique.[17,18] The LB technique is a valuable technique for preparing thin films as it enables (i) the precise control of the monolayer thickness, (ii) homogeneous deposition of the monolayer over large areas, and (iii) the possibility to make multilayer structures with varying layer composition. Amphiphilic long-chain fluorophores deposited by the LB technique are expected to be at one distance rather than a range of distances from the metal surface or the metal island films, but of course there will still be in-plane heterogeneity of fluorophores on or between the silver particles. Considering this, we have synthesized long-chain nitrobenzoxadiazole (NBD) derivatives having two different alkyl chain lengths (NBD-C18 and NBD-C16) for the preparation of LB monolayers. NBD probes show unique spectral properties, including high quantum yields and large Stokes shift suitable for the present study.[19−21] In this paper, we investigate the MEF of NBD-C16 and NBD-C18 monolayers on the SIF substrates. This study has been undertaken to reveal the metal nanoparticle and fluorophore interaction in the organized molecular film systems. We also present the modulations in MEF with respect to the changes in microenvironment polarity and surface plasmon resonance.

Experimental Details

Materials and Methods. Long-chain alkylamines (hexadecylamine and octadecylamine), 4-chloro-7-nitrobenz-2-oxa-1,3-diazole (NBD-Cl), stearic acid (SA), and spectroscopic grade chloroform were obtained from Aldrich and used without further purification. Distilled water, purified with the Millipore Milli-Q Gradient System, was used for LB monolayer deposition and in all other chemical modifications. All other compounds, including silver nitrate, ammonium hydroxide, sodium hydroxide, and glucose were purchased from Sigma-Aldrich (St. Louis, MO) and used as received.

Synthesis of Nitrobenzoxadiazole (NBD) Derivatives. The molecular structures of the newly designed probes NBD-C16 [(4-hexadecylamino)-7-nitrobenz-2-oxa-1,3-diazole] and NBD-C18 [(4-octadecylamino)-7-nitrobenz-2-oxa-1,3-diazole] used in this study are shown in Figure 1. These compounds were prepared by using a generic one-step synthetic procedure as described below for NBD-C16. We simply used the corresponding amount of octadecylamine instead of hexadecylamine to obtain NBD-C18. The acetonitrile (5 mL) solution of NBD-Cl (0.200 g, 1 mmol) and hexadcylamine (0.265 g, 1.1 mmol) in a 25-mL round-bottom flask equipped with an air condenser and a gas outlet was stirred continuously overnight with a magnetic stirrer at room temperature. After completion of the reaction, the orange precipitate was filtered and washed several times with excess acetonitrile and the solid product was purified by using a neutral alumina coloumn. The pure product was obtained by eluting with a 50:50 hexane:ethyl acetate mixture of solvents (yields ∼95%). The NMR and high-resolution mass spectral data of both compounds, as shown below, are in accordance with the molecular structure of the probes.

Spectral data for NBD-C16: ^{1}H NMR ($CDCl_3$, δ, ppm) 0.879 (t, 3H), 1.2−1.5 (m, 26H), 1.8 (quintet, 2H), 3.5 (quartet, 2H), 6.19 (d, 1H), 6.23 (s, 1H), and 8.5 (d, 1H). ^{13}C NMR ($CDCl_3$, δ, ppm) 14.0 (1C), 23.0 (1C), 26.0 (1C), 29.0 (1C), 29−30 (10C), 32.0 (1C), 44 (1C), 141.1 (1C), 141.6 (1C), 142.0 (1C) 148.0 (1C), and 150 (1C). HRMS (FAB+, ethyl acetate) *m*/*e* calcd 404.2787 (M^+), found 404.2687 (M^+).

Spectral data for NBD-C18: ^{1}H NMR ($CDCl_3$, δ, ppm) 0.879 (t, 3H), 1.2−1.5 (m, 30H), 1.8 (quintet, 2H), 3.5 (quartet, 2H), 6.19 (d, 1H), 6.21 (s, 1H), and 8.5 (d, 1H). ^{13}C NMR ($CDCl_3$, δ, ppm) 14.2 (1C), 23.5 (1C), 26.0 (1C), 29.0 (1C), 29−30 (12C), 32.0 (1C), 44 (1C), 141.1 (1C), 141.6 (1C), 142.0 (1C) 148.0 (1C), and 150 (1C). HRMS (FAB+, ethyl acetate) *m*/*e* calcd 432.5994 (M^+), found 432.5989 (M^+).

Silver Island Film (SIF) Preparation. The glass slides (Corning, NY) used for silver island film (SIF) preparation were first cleaned by soaking them overnight in a 10:1 (v/v) mixture of H_2SO_4 (95−98%) and H_2O_2 (30%), commonly known as piranha (*Warning*: *piranha solution reacts strongly with organic compounds and should be handled with extreme caution*; *do not store the solution in closed containers*). After being washed rigorously with MilliQ deionized water, the glass slides were air-dried. SIFs were deposited on clean glass slides using the method reported previously by us.[22] Briefly, about 1.5 mL of freshly prepared 5% NaOH solution was added to a stirring aqueous silver nitrate solution (0.375 g in 45 mL of water) in a glass beaker. Subsequently, the resulting dark-brown precipitate was redissolved by slowly adding 1 mL of NH_4OH. The solution was cooled to 5 °C in an ice bath and a fresh solution of D-glucose (0.540 g in 11 mL of water) was added, followed by four pairs of dried glass slides placed into this solution. The mixture was stirred for 2 min in an ice bath and then allowed to warm to 30 °C for the next 5 min. As the color of the mixture turned from yellow-greenish to yellow-brown, the color of the slides became greenish. The slides were removed from the beaker and rinsed with Milli-Q water. Excess and nonadhesive silver particles on the glass surface were removed by mild sonication of the SIF coated glass slides for 1 min. As the result of using a sandwiched glass pair for SIFs formation, only one side of each slide was coated with silver islands. The SIF slides were stored in Milli-Q water until they were used for LB deposition. SIFs displayed the characteristic surface plasmon resonance with an absorption maximum near 460 nm.

LB Film Deposition. LB film depositions on solid substrate are accomplished with use of computer controlled KSV 5000 LB trough. Milli-Q deionized water (pH ∼5.8 at 20 °C, with resistivity of 18.2 MΩ·cm) was used as the water subphase. The probe monolayers on the water subphase were formed by spreading the known concentration of NBD-C16 or NBD-C18 in chloroform. To obtain NBD−stearic acid mixed monolayers, various molar ratios of SA and NBD probes were dissolved in chloroform and used for the monolayer preparation on the water subphase. After allowing 15 min to evaporate the chloroform, the monolayer at the air−water interface was slowly compressed to a surface pressure of 20 mN/m. Subsequently, the compressed monolayer was transferred by the LB technique onto the solid

substrates, where a clean glass and SIFs coated glass slides were sandwiched together and monolayers were deposited at a dipping speed of 5 mm/min during the upstroke. The observed monolayer transfer ratio from the compressed water subphase to substrate was ~0.95.

Absorption and Fluorescence Spectroscopy. Absorption spectra were collected with a Hewlett-Packard 8453 spectrophotometer. Fluorescence spectra of monolayers on solid substrates were recorded with a Varian Cary Eclipse fluorescence spectrophotometer, using front face illumination geometry with 470 nm excitation from a Xenon arc lamp. Time-resolved intensity decays were recorded with a PicoQuant Fluotime 100 time-correlated single-photon counting (TCSPC) fluorescence lifetime spectrometer. The excitation at ~470 nm was obtained by using a pulsed laser diode (PicoQuant PDL800-B) with a 20 MHz repetition rate. The Instrument Response Function (IRF) is about 300 ps. The excitation was vertically polarized and the emission was recorded through a polarizer oriented at 54.7° from the vertical position. A band-pass filter at 530−585 nm (Chroma Inc.) was used in the collection path, thus eliminating the scattered excitation light and collecting the fluorescence from the NBD probes in the region of interest.

Data Analysis. The fluorescence intensity decays were analyzed in terms of the multiexponential model as the sum of individual single exponential decays:[23]

$$I(t) = \sum_{i=1}^{n} \alpha_i \exp(-t/\tau_i) \quad (1)$$

In this expression τ_i are the decay times and α_i are the amplitudes and $\sum_i \alpha_i = 1.0$. The fractional contribution of each component to the steady-state intensity is described by:

$$f_i = \frac{\alpha_i \tau_i}{\sum_j \alpha_j \tau_j} \quad (2)$$

The average lifetime is represented by

$$\bar{\tau} = \sum_i f_i \tau_i \quad (3)$$

The values of α_i and τ_i were determined by using the PicoQuant Fluofit 3.3 software with the deconvolution of instrument response function and nonlinear least-squares fitting. The goodness-of-fit was determined by the χ^2 value.

Results and Discussion

Photophysical Properties of the Probes in Solution. The probes NBD-C16 and NBD-C18 shown in Figure 1 are conveniently prepared in quantitative yields. The NBD derivatives are known to display broad absorption and emission bands devoid of any fine structure due to the intramolecular charge transfer (ICT) nature of ground and excited states, respectively.[19−21] The ICT nature of these probes is evident from the solvatochromic response of the absorption and fluorescence spectra of the compounds in several solvents (Figure 2). As seen from the figure, with an increase in the polarity of the solvent, the fluorescence band maximum exhibits a gradual bathochromic shift, 505 nm in ether to 534 nm in methanol. The corresponding shift in the absorption spectra is relatively less (from 446 nm in ether to 467 nm in methanol), indicative of a more polar excited state over the ground state.[19−21,23] Both derivatives, NBD-C16 and NBD-C18, show very similar spectral properties in all the solvents (data not shown), giving no importance to the difference in appending alkyl chain length. On the basis of these interesting features of the probes, we anticipate these probes are suitable to explore the effect of local polarity and overall electron density of the SIFs surface on the net MEF efficiency.

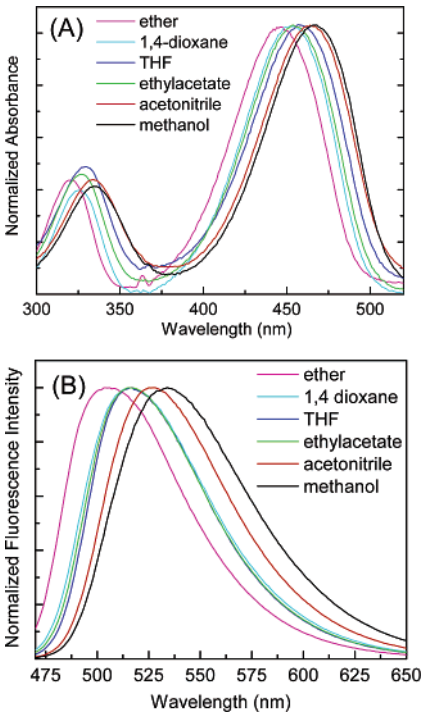

Figure 2. Normalized absorption (A) and fluorescence emission (B) spectra of NBD-C18 in different solvents.

Spectral Properties of the Probes on a Glass Surface. Monolayers of the probes were deposited on a glass surface at a surface pressure of 20 mN/m and used immediately for spectral measurements. The absorption and fluorescence emission spectra of the NBD-C18 monolayer on a glass slide are shown in Figure 3. For easy comparison we have shown again the corresponding spectra of the probe in methanol (Figure 3B). Interestingly, the absorption spectrum of the monolayered NBD probe on glass shows a peak at about 515 nm and a shoulder at 540 nm, and both absorption and fluorescence bands are red shifted when compared to that in methanol. This red shift may not be explained just based on the polarity increase from methanol to glass but it also may be partially due to the extended intermolecular interactions between the closely packed NBD probes. A schematic representation of probe alignment on the solid substrate is shown in Figure 4 (vide infra). To reduce the intermolecular interactions we deposited mixed LB monolayers of NBD and stearic acid. But we have not seen any noticeable change in the shape and position in the absorption spectra even when we used 4 times diluted probe (Figure 5), except the lowered overall optical density of the film. On the other hand, a consistent reduction in fluorescence intensity and blue shift in band maximum is noticed with the same dilution. The observed reduction can be simply ascribed to the probe dilution in the film, and the blue shift in the emission band was the result of two factors: the first one could be the reduced intermolecular interactions and the second is reduction in polarity in diluted mixed monolayers. The emission band maximum of mixed monolayers of NBD probes (NBD-C*x*:SA = 1:3) shows a band maximum at 530 nm ,which is consistent with the previously published results.[24]

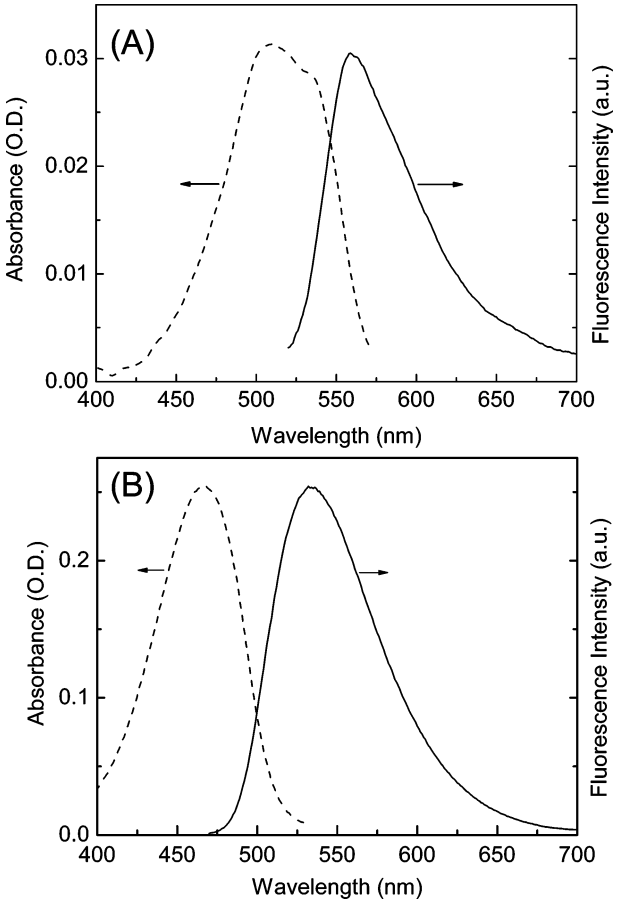

Figure 3. Absorption and emission spectra of a NBD-C18 monolayer on glass (A) and in methanol (B).

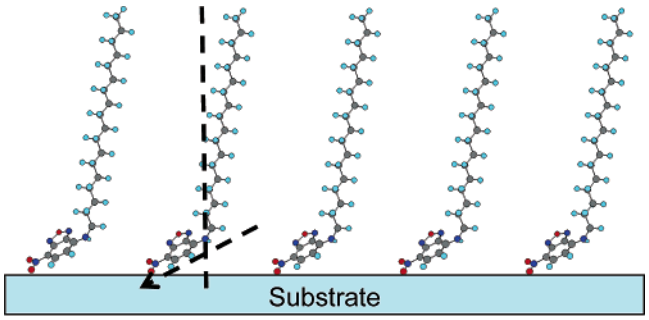

Figure 4. Schematic representation of a NBD-C18 monolayer on glass or SIFs. The vertical dashed line indicates the vertical plane with respect to the surface normal and the dashed arrow shows the probe dipole orientation with respect to the plane of the surface. The probe structure was energy minimized by using AM1 calculations, provided with ChemDraw Ultra.

NBD Probe Packing and Orientation in the LB Monolayer. Polarized visible absorption[25−27] or infrared attenuated total reflection spectra[28] can provide an indication of the order and orientation of the LB films deposited on solid substrates. Accordingly, in the present case, the absorption spectra of NBD-C16 and NBD-C18 molecules in LB monolayers from the $S_1 \leftarrow S_0$ transition are sensitive to the direction of polarization of incident light, which enables the use of polarized light to probe the structural anisotropy within the LB monolayer films. The electric vector (polarization direction) of the incident radiation is perpendicular and parallel to the dipping direction. Figure 6 illustrates the absorption spectra measured for LB monolayers of NBD-C18 on a glass slide (only one side of the substrate) at two incident angles. At the normal incidence the absorption

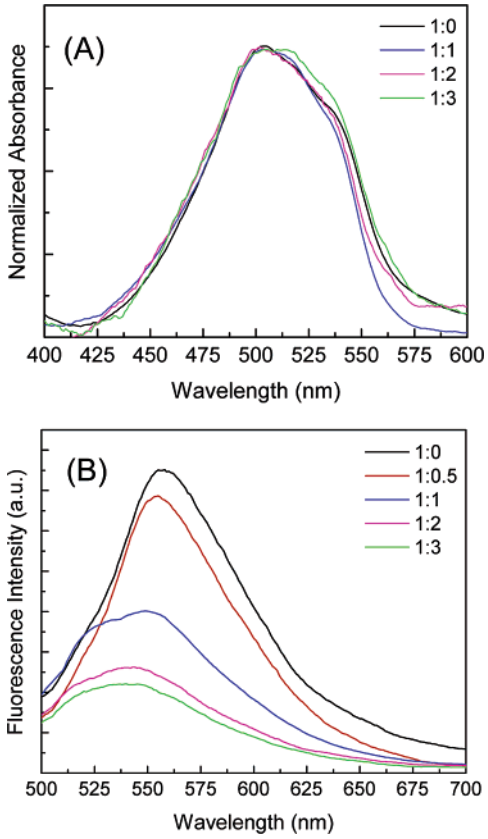

Figure 5. (A) Normalized absorption spectra of monolayers of NBD-C16:SA with different molar ratios on glass and (B) emission spectra from the corresponding monolayers.

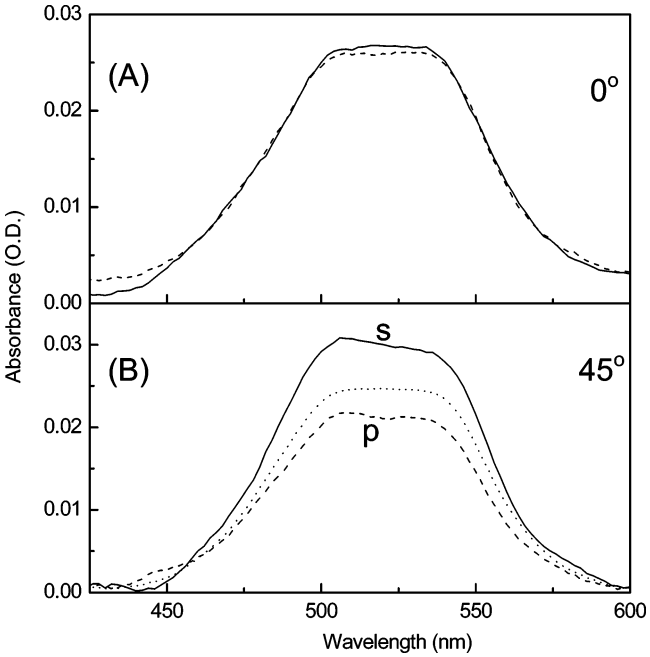

Figure 6. Polarized absorption spectra of the NBD-C18 monolayer at the incidence angle of 0° (A) and 45° (B). Solid and dashed lines indicate the absorption spectra for s- and p-polarized light, respectively. The dotted line in bottom panel indicates the spectra for unpolarized light.

intensities for the p- and s-polarized lights are almost the same. This suggests that the vectors of the transition dipole moments of the NBD molecules are uniformly distributed over the film surface, taking a constant angle with the surface normal. On the other hand, when the film was tilted 45°, the absorption

under the s-polarization mode is stronger than that of the p-polarization; the unpolarized absorption falls between the two extremes. A quantitative evaluation of the molecular orientation of the NBD-C18 molecule was made by considering four phases, namely air, LB film, substrate, and air. Assuming a uniaxial orientation of the transition dipole moment with the angle θ, the ratio between p- and s-polarized intensities is given by eq 4[29−31]

$$\frac{A_p}{A_s} = \frac{n_1 \cos i + n_3 \cos r}{n_2 \cos r + n_3 \cos i}\left\{\cos i \cos r + \frac{2{n_1}^3 n_3 \sin^2 i}{{n_2}^4 \tan^2 \theta}\right\} \quad (4)$$

where the refractive indices of four phases are assumed to be $n_1 = 1.00$ (air), $n_2 = 1.50$ (LB film), and $n_3 = 1.54$ (substrate), i is the angle of incidence at the LB film, and r is the angle of refraction at the interface of the LB film and substrate that can be evaluated from $n_1 \sin i = n_3 \sin r$. θ is the tilt angle of the transition dipole moment of the NBD probe molecule with respect to the surface normal. From the above equation we calculated the tilt angle, θ, of 67.3° for the NBD-C18 molecule in the monolayer LB film. Since the direction of transition moment of the NBD-C18 molecule is assigned along the short axis (amino nitrogen to nitro group), this measurement suggests that the short axis of the NBD-C18 molecule tilted considerably from the surface normal as shown schematically in Figure 4. We have not observed any significant change in the tilt angle for NBD-C18 molecules in the NBD:stearic acid mixed monolayers and the value of θ lies between 67° and 68°. The estimated tilt angles for the NBD-C16 molecules in pure monolayer and in mixed monolayers are also very similar to those obtained with NBD-C18.

Metal Enhanced Fluorescence. The fluorescence emission spectra of the NBD-C18 LB monolayer on a glass slide and SIFs are presented in Figure 7. LB monolayer deposited on glass slides is used as a reference sample to estimate the metal effect, i.e., MEF. The fluorescence spectra were collected at the same excitation and detection conditions allowing a direct comparison between the two substrates. The normalized fluorescence spectra of monolayers of NBD-C18 on both glass and SIFs are shown in the inset of Figure 7. Interestingly, as shown in Figure 7, the emission spectra from the metalized and that from the nonmetalized area completely overlap on each other with a band maxima at about 560 nm. A very similar response was also noticed with NBD-C16 on both substrates. Subsequently, from the inset of Figure 7 one can assume that the organized monolayer pattern and intermolecular interactions between the closely packed probes on glass and SIF surfaces are very similar and the difference in the emission intensity is not due to the difference in the local polarities of the glass and SIFs surface. A significant enhancement (of about 16-fold) in fluorescence intensity is observed from the monolayers of NBD on SIFs as compared to that on the glass surface (Figure 7). The factor of fluorescence enhancement can be defined as a ratio of integrated intensities detected on SIFs and glass substrates in the 520−700 nm spectral range. The observed fluorescence enhancement from NBD monolayers deposited on SIFs seems surprising considering the usual expectations of fluorescence quenching when the probes are placed directly on the metal surface. Normally, it is suggested that a 5 to 10 nm spacer layer is required to avoid quenching.[4] To understand this unusual observation we spin coated the comparable concentration of the NBD-C18 solution onto both glass and SIFs, and used these for MEF experiments. Interestingly, the observed MEF from the spin coated slides is considerably less (2.5-fold MEF, Figure 7B) when compared to that from the LB monolayer (16-fold MEF). Overall, it seems surprising that the largest enhancement was observed when the fluorophore was placed directly on the SIFs.

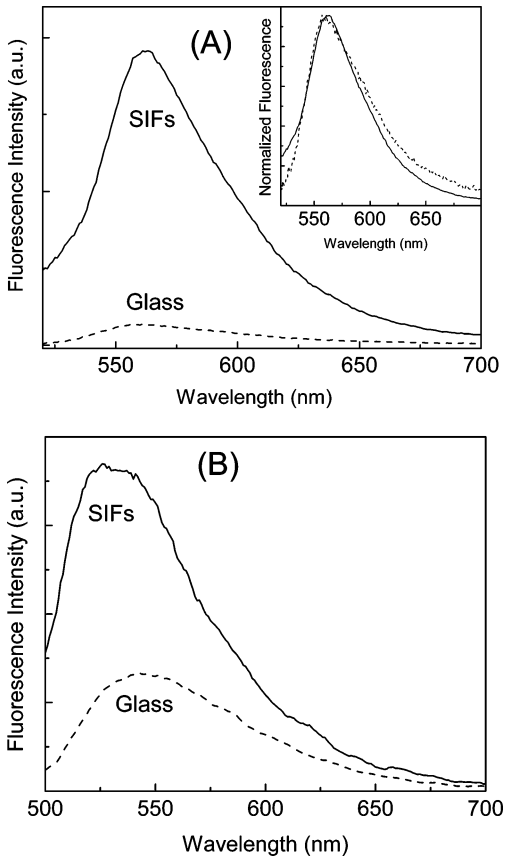

Figure 7. (A) Emission spectra of a LB monolayer of NBD-C18 on glass and SIF surface; the inset shows the corresponding intensity normalized emission spectra. (B) Emission spectra of a NBD-C18 layer on glass and SIFs obtained by using the spin coating method.

The emission of fluorophores near the silver nanostructures is dependent on at least two factors: an enhanced local field and an increase in the intrinsic decay rate of the fluorophore due to MEF.[4,16] The first factor provides stronger excitation rates. The second factor changes the quantum yield and lifetime of the fluorophore. The radiative decay rate modification of the NBD derivatives in close proximity to the silver nanostructures is consistent with the previous reports on the MEF phenomenon and due to the proximity of the fluorophores to the silver nanostructures.[1−12] The increase in local field results in a higher excitation rate but does not modify the fluorescence lifetime of the molecules.

An increase in the rate of radiative decay yields shorter lifetimes. To verify this effect we have measured the time-dependent intensity decays of LB monolayers of NBD derivatives using a time correlated single photon counting (TCSPC) instrument.[23] The fluorescence intensity decay curves of NBD-C18 monolayer deposited on a glass substrate and SIF are shown in Figure 8. Also shown in the figure is the instrument response function. The solid lines indicate the best fit to the experimental decay curves. A very similar decay response is noticed with NBD-C16. As can be seen from the figure, the intensity decay of NBD monolayers on SiFs is faster than those on the glass substrate. The fluorescence lifetime of NBD derivatives is significantly (of ∼1.7-fold) shortened when the monolayers are on the SiF. This shortening of lifetime on SiFs strongly supports that the increase in fluorescence intensity is due to the presence

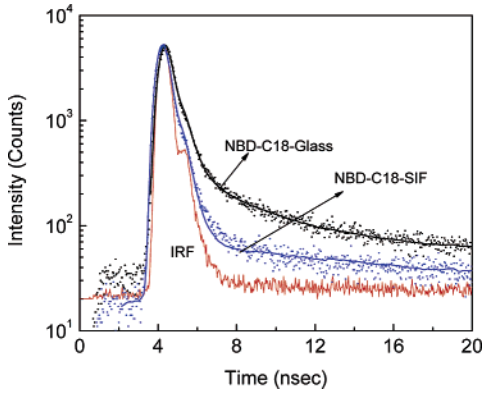

Figure 8. Fluorescence intensity decays of a monolayer of NBD-C18 on glass and SIFs. The instrument response function (IRF) is also included.

of the fluorophores near the silver nanoparticles.[1−12] We have verified that the short component in the intensity decay is not due to scattered light. Metallic colloids are known to scatter strongly.[32−34] Control measurements on the glass or SiF substrates, without NBD derivatives, yielded a very weak signal when observed through the combination of filters used to isolate the NBD emission. We further examined the possibility of scattered light by recording the emission spectra through the emission filter sets used for the intensity−time decay measurements. These spectra showed very weak intensity at the excitation wavelength of 470 nm, demonstrating that scattered light is not the origin of the short lifetime components of NBD derivatives on SiFs.

The simultaneous increase of quantum efficiency and decrease of lifetime indicates an increased radiative decay rate in the presence of silver particles.[1] The quantum yield and lifetime of a fluorophore are interrelated as defined below:

$$\Phi_0 = \frac{\Gamma}{\Gamma + k_{nr}} \tag{5}$$

$$\tau_0 = \frac{1}{\Gamma + k_{nr}} \tag{6}$$

where Γ and k_{nr} are the radiative and nonradiative decay rates, respectively. In the presence of metal, the quantum yield and lifetime are given by

$$\Phi_m = \frac{\Gamma + \Gamma_m}{\Gamma + \Gamma_m + k'_{nr}} \tag{7}$$

$$\tau_m = \frac{1}{\Gamma + \Gamma_m + k'_{nr}} \tag{8}$$

where Γ_m and k'_{nr} are radiative and nonradiative rates in the presence of metal particles. Increases in radiative rates near SIFs result in increased quantum yields and decreased lifetimes. The modifications of k_{nr} by metal are assumed to be negligible. The above equations result in the unusual prediction for fluorophore−metal interactions that the lifetime decreases as the intensity increases.[4,23] This unusual effect is due to a change in the radiative decay rate of the fluorophores, which depends on the photonic mode density near the fluorophore[4] and seems responsible for the observed 16-fold enhancement in fluorescence and shortened fluorescence lifetime of LB monolayeres on SIFs.

MEF from the Mixed LB Monolayers of NBD Derivatives. The NBD probes are known for their solvent sensitivity (Figure 2). Accordingly, we anticipated that the dilution of NBD monolayers with nonpolar amphiphilic entities such as stearic acid may alter the spectral properties (as shown in Figure 5), and the net MEF from the probes on SIFs. Figure 9 presents the normalized fluorescence emission spectra of mixed monolayers of NBD-C16 and NBD-C18 on SIFs with varying molar composition of SA. With addition of more fatty acid, the emission peak is blue-shifted as was observed on the glass surface (Figure 5B). It is important to note here that the emission spectra of one particular mixed monolayer (for example, NBD:SA with a molar ratio of 1:3) on either SIFs or a glass surface can overlap on each other as shown earlier for the NBD-C18 monolayer (inset of Figure 7). This again substantiates that the local microenvironment, monolayer composition, and intermolecular interactions in the closely packed probes in the LB layers on the glass and SIFs coated glass surface are very similar, and the observed blue shift is primarily due to the polarity change resulting from the dilution.

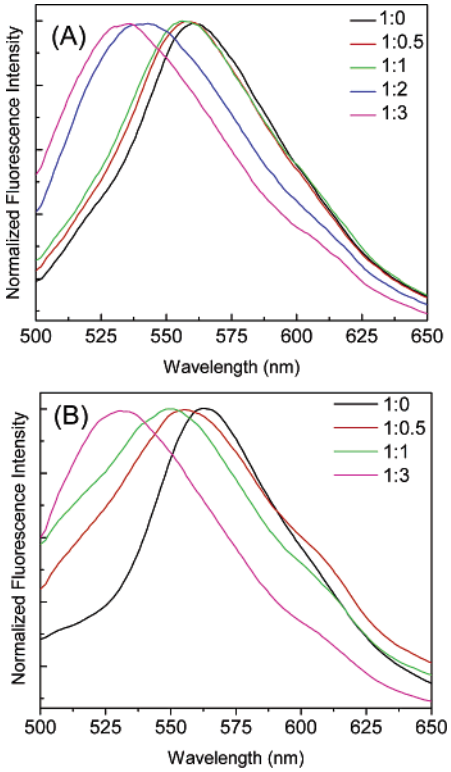

Figure 9. Normalized emission spectra of monolayers of NBD-C16 (A) and NBD-C18 (B) with various molar ratios of SA on SIFs.

Subsequently, the observed fluorescence spectral shift along with the increase in MEF for mixed monolayers are represented as histograms (Figure 10), where the left panel in the figure indicates the emission band maxima and the right panel denotes the MEF efficiency with respect to varying molar ratios of SA. A very similar hypsochromic shift of 30 nm in the fluorescence band maxima is observed for both NBD-C16 and NBD-C18 probes. Most importantly, as shown in the figure, MEF efficiency is increased from 16- to 32-fold when moving from the pure NBD monolayer to the NBD:SA mixed monolayer with a 1:3 molar ratio. The increase in MEF efficiency is difficult to understand at this time. But we consider there may be several known and unknown parameters contributing to the net MEF from the probes. Among these parameters, probe orientation[35,36] and the local electron density in the surface plasmon band[37] and subsequent effects of refractive index[38−42] and/or ligand[43−45] alterations in plasmon electron density may contribute to the net MEF for the organized monolayer system.[4]

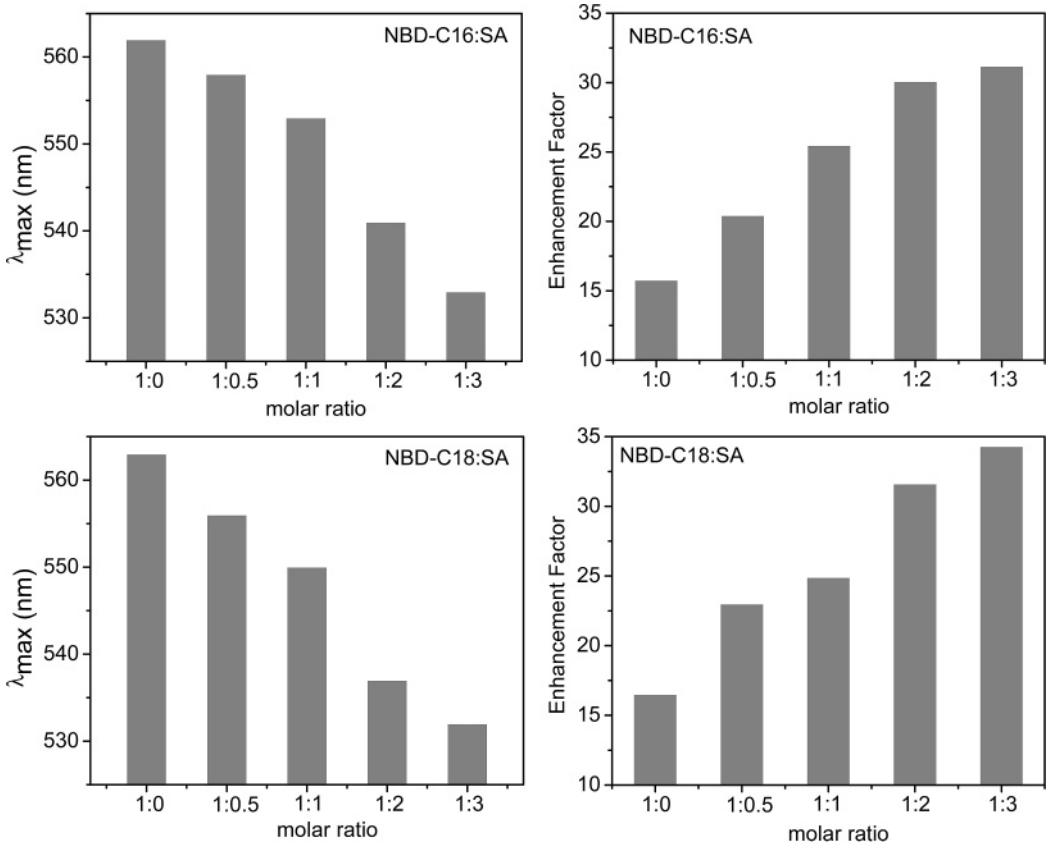

Figure 10. Histograms of λ_{max} (left) and fluorescence enhancement factor (right) for various molar ratios of NBD-C16 (top panel) and NBD-C18 (bottom panel) with SA.

To understand the LB monolayer induced modulations in the localized surface plasmon resonance of the silver island film, we measured the plasmon absorption spectra of the pure NBD monolayer and mixed monolayers on SIFs and compared them with that of bare SIFs (Figure 11). As shown in the figure, SIFs show characteristic absorption with a band maximum at 460 nm. A considerable blue shift in the surface plasmon band is noticed with the pure NBD monlayer, whose band maximum is at 435 nm. On the other hand, the plasmon absorption band maximum of mixed monolayers of NBD:SA shows a gradual red shift, with the total shift of ∼20 nm for the NBD:SA monolayer with a 1:3 molar ratio. Figure 11B shows the effect of the NBD:SA molar ratio on the surface plasmon absorption band position. The observed shift can be explained based on the well-described ligand stabilization effect on surface plasmon resonance. For example, a similar shift is known for the oxyanion binding to the silver surface in the literature.[45] Further, it is interesting to note that the probe layer obtained by spin coating the methanol solution of NBD-C18 on SIFs has very little effect on the surface plasmon band: only ∼5 nm blue shift in the plasmon absorption band is noticed with SIFs having the spin coated probe, whereas the corresponding shift for SIFs with the LB film is 30 nm (Figure 11). This clearly indicates the probe interaction with the metallic surface is increased considerably for the organized monolayers, and minute modulations in the fluorophore−metal interactions may lead to significant changes in the net output fluorescence intensity, i.e., MEF efficiency in the system. Additionally, the fluorophores in the oriented films may be preferentially excited contributing to the higher MEF efficiency, whereas such preferential excitation of the probes in spin coated films is less effective.

To understand the increased MEF from 16- to 32-fold when moving from the NBD pure monolayer to the NBD:SA (1:3)

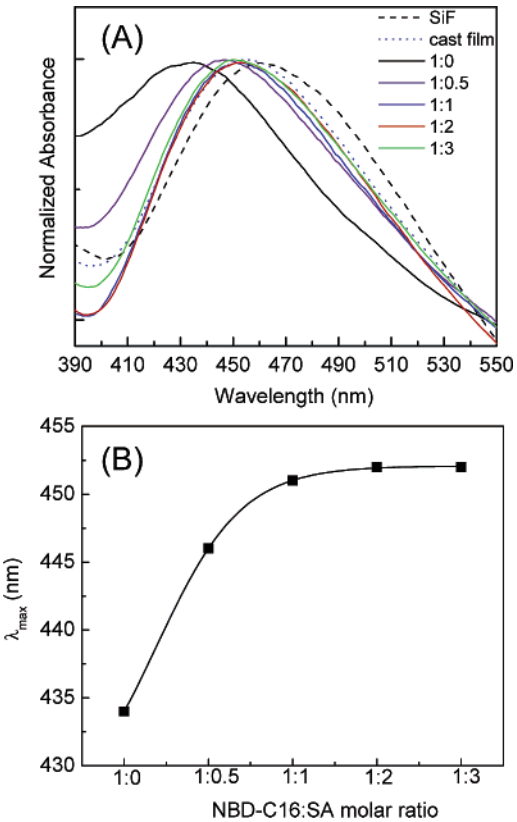

Figure 11. (A) Normalized surface plasmon absorption spectra of SIFs, NBD-C16 spin coated on SIFs, and LB monolayers of NBD-C16 and SA at different molar mixing ratios on SIFs. (B) Change in peak position of the localized surface plasmon resonance band with molar ratio of probe and SA.

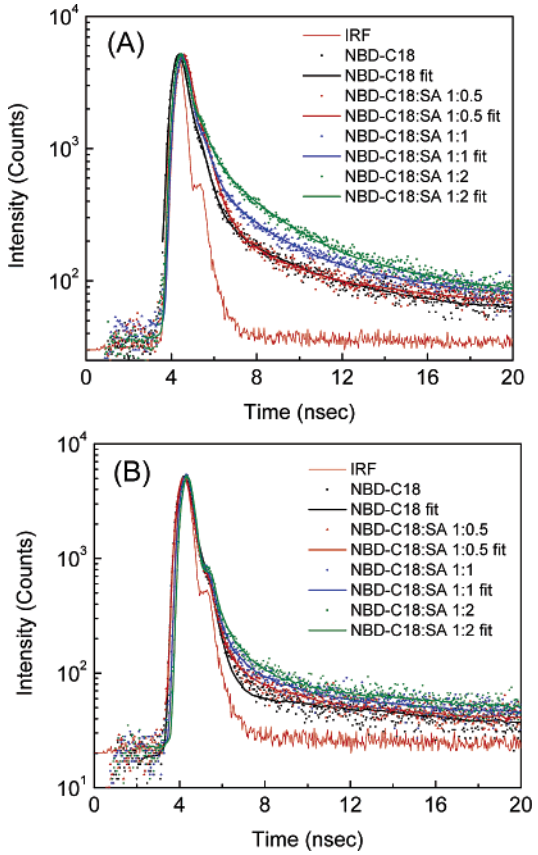

Figure 12. Fluorescence intensity decays of NBD-C18 pure and mixed monolayers on glass (A) and SIFs (B) surfaces. The instrument response function (IRF) is also included.

mixed monolayer, we also measured the fluorescence intensity decays for each mixed monolayer of both NBD-C16 and NBD-C18. Representative intensity decays obtained for the NBD-C18 monolayer on glass and SIFs surfaces are shown in Figure 12. As can be seen from the figure the fluorescence intensity decays of the probes on glass show a steady increase in the average lifetime (from 0.3 ns for NBD-C18 pure monolayer on glass to 0.5 ns for NBD-C18:SA (1:2) mixed monolayer). Although the magnitude of this lifetime increase is very small, it is interesting to compare the intensity decays of the corresponding mixed monolayers on SIFs surface (Figure 12B), where there is no significant change in the lifetimes of the probes on SIFs surface. As stated earlier, we observed about a 1.7-fold reduction in the average lifetime for NBD pure monolayer on SIFs surface when compared to that on glass and this factor was consistently increased with increasing fatty acid composition in the monolayer and about a 4-fold decrease in average lifetime is observed for the NBD:SA (1:3) mixed monolayer on SIFs. This consistent decrease in lifetime with the dilution of the probe concentrations in the monolayer further emphasizes that the increased MEF for the mixed monolayers of the probes is in accordance with our so-called MEF phenomenon.

Conclusions

We reported here in this article a 16-fold MEF from well-organized, oriented, and closely packed long-chain NBD probes on silver island films deposited with use of the Langmuir−Blodgett technique. We have obtained more detailed information on metal−fluorophore interactions resulting from MEF by having defined the probe distance and orientation with respect to the metal surface. We have successfully observed significant MEF from the probe monolayer with contacting the distance from the surface and with a 67−68° tilt angle with respect to surface normal. We compared the MEF results obtained using LB films with those of spin coated probes on glass and the results emphasize the importance of organized, oriented films for improved MEF effects. Subsequently we addressed briefly the effect of dilution on pure monolayers with the amphiphilic stearic acid on both the spectral properties of the probes and the MEF. We observed increased MEF of about 32-fold from the mixed monolayer (NBD:SA = 1:3) and further reduction in lifetimes, which is quite significant toward fine-tuning the MEF efficiency.

Acknowledgment. The present work was supported by the National Institute of Health (NIH), The Center for Research Resources, RR-08119.

References and Notes

(1) Lakowicz, J. R. *Anal. Biochem*. **2001**, *298*, 1−24.
(2) Lakowicz, J. R.; Shen, Y.; D'Auria, S.; Malicka, J.; Fang, J.; Grcyzynski, Z.; Gryczynski, I. *Anal. Biochem*. **2002**, *301*, 261−277.
(3) Lakowicz, J. R. *Anal. Biochem*. **2004**, *324*, 153−169.
(4) Lakowicz, J. R. *Anal. Biochem*. **2005**, *337*, 171−194.
(5) Lakowicz J. R.; Shen Y.; Gryczynski Z.; D'Auria S.; Gryczynski I. *Biochem. Biophys. Res. Commun.* **2001**, *286*, 875−879.
(6) Aslan, K.; Gryczynski I.; Malicka J.; Matveeva E.; Lakowicz, J. R.; Geddes, C. D. *Curr. Opin. Biotechnol.* **2005**, *16*, 55−62.
(7) Aslan, K.; Lakowicz, J. R.; Geddes, C. D. *Curr. Opin. Chem. Biol.* **2005**, *9*, 538−544.
(8) Lakowicz, J. R.; Chowdhury, M. H.; Ray, K.; Zhang, J.; Fu, Y.; Badugu, R.; Sabanayagam, C. R.; Nowaczyk, K.; Szmacinski, H.; Aslan, K.; Geddes, C. D. *Proc. SPIE* **2006**. In press.
(9) Lakowicz J. R.; Malicka J.; D'Auria S.; Gryczynski I. *Anal. Biochem.* **2003**, *320*, 13−20.
(10) Aslan, K.; Lakowicz, J. R.; Geddes, C. D. *Anal. Bioanal. Chem.* **2005**, *382*, 926−933.
(11) Geddes, C. D.; Aslan, K.; Gryczynski, I.; Malicka, J.; Lakowicz, J. R. In *Annual Reviews in Fluorescence 2004*; Geddes, C. D., Lakowicz, J. R., Eds; Kluwer Academic/Plenum Publishers: New York, 2004; pp 365−401.
(12) Geddes, C. D.; Aslan, K.; Gryczynski, I.; Malicka, J.; Lakowicz, J. R. In *Topics in Fluorescence Spectroscopy*; Geddes, C. D., Lakowicz, J. R., Eds.; Kluwer Academic/Plenum Publishers: New York, 2005; pp 401−448.
(13) Weitz, D. A.; Garoff, S.; Hanson, C. D.; Gramila, T. J.; Gersten J. I. *Opt. Lett.* **1982**, *7* (2), 89−91.
(14) Wokaun, A.; Lutz, H.-P.; King, A. P.; Wild, U. P.; Ernst, R. R. *J. Chem. Phys.* **1983**, *79* (1), 509−513.
(15) Malicka, J.; Gryczynski, I.; Kusba, J.; Lakowicz, J. R. *Biopolymers* **2003**, *70*, 595−603.
(16) Lakowicz, J. R. *Plasmonics*. In press.
(17) Ulman, A. *An introduction to ultrathin organic films*: *from Langmuir−Blodgett to self-assembly*; Academic Press: San Diego, CA, 1991.
(18) Ashwell, G. J.; Hargreaves, R. C.; Baldwin, C. E.; Bahra, G. S.; Brown, C. R. *Nature* **1992**, *357*, 393.
(19) Saha, S.; Samanta, A. *J. Phys. Chem. A* **1998**, *102*, 7903−7912.
(20) Chattopadhyay, A. *Chem. Phys. Lipids* **1990**, *53*, 1.
(21) Mukherjee, S.; Chattopadhyay, A.; Samanta, A.; Soujanya, T. *J. Phys. Chem.* **1994**, *98*, 2809−2812.
(22) Malicka, J.; Gryczynski, I.; Lakowicz, J. R. *Biochem., Biophys. Res. Commun.* **2003**, *306*, 213−218.
(23) Lakowicz, J. R. *Principles of Fluorescence Spectroscopy*, 2nd ed.; Kluwer Academic/Plenum Publishers: New York, 1999.
(24) Yu, Q.; Vuorimaa, E.; Tkachenko, N. V.; Lemmetyinen, H. *J. Lumin.* **1997**, *75*, 245−253.
(25) Nakahara, H.; Fukuda, K. *J. Colloid Interface Sci*. **1981**, *83*, 401.
(26) Nakahara, H.; Fukuda, K. *J. Colloid Interface Sci*. **1984**, *98*, 555.
(27) Kawai, T.; Umemura, J.; Takenaka, T. *Langmuir* **1989**, *5*, 1378.
(28) Kimura, F.; Umemura, J.; Takenaka, T. *Langmuir* **1986**, *2*, 96.
(29) Vandevyer, M.; Barraud, A.; Texier, R.; Maillard, P.; Giannotti, C. *J. Colloid Interface Sci.* **1882**, *85*, 571.
(30) Chollet, R. A. *Thin Solid Films* **1978**, *52*, 343.
(31) Stanescu, M.; Samha, H.; Peristein, J.; Whitten, D. G. *Langmuir* **2000**, *16*, 275.

(32) Yguerabide, J.; Yguerabide, E. E. *Anal. Biochem.* **1998**, *262*, 137−156.
(33) Yguerabide, J.; Yguerabide, E. E. *Anal. Biochem.* **1998**, *262*, 157−176.
(34) Schultz, S.; Smith, D. R.; Mock, J. J.; Schultz, D. A. *Proc. Natl. Acad. Sci.* **2000**, *97*, 996−1001.
(35) Ishida, A.; Majima, T. *Chem. Commun.* **1999**, 1299−1300.
(36) Ishida, A.; Sakata, Y.; Majima, T. *Chem. Commun.* **1998**, 57−58.
(37) Hutter, E.; Fendler, J. H. *Adv. Mater.* **2004**, *16*, 1685−1706.
(38) Mulvaney, P. *Langmuir* **1996**, *12*, 788−800.
(39) Underwood, S.; Mulvaney, P. *Langmuir* **1994**, *10*, 3427−3430.
(40) Templeton, A. C.; Pietron, J. J.; Murray, R. W.; Mulvaney, P. *J. Phys. Chem. B* **2000**, *104*, 564−570.
(41) Malinsky, M. D.; Kelly, K. L.; Schatz, G. C.; Van Duyne R. P. *J. Am. Chem. Soc.* **2001**, *123*, 1471−1482.
(42) Stuart, D. A.; Haes, A.; McFarland, A. D.; Nie, S.; Van Duyne, R. P. *Proc. SPIE* **2004**, *5327*, 60−73.
(43) Ghosh, S. K.; Nath, S.; Kundu, S.; Esumi, K.; Pal, T. *J. Phys. Chem. B* **2004**, *108*, 13963−13971.
(44) Linnert, T.; Mulvaney, P.; Henglein, A. *J. Phys. Chem.* **1993**, *97*, 679−682.
(45) Cumberland, S. L.; Strouse, G. F. *Langmuir* **2002**, *18*, 269−276.